Diffraction paradox: An unusually broad diffraction background marks high quality graphene

S. Chen,[1,2] M. Horn von Hoegen,[4] P. A. Thiel,[1,3] and M. C. Tringides[1,2,*]

[1]*Ames Laboratory - U.S. Department of Energy, Ames, Iowa 50011, USA*
[2]*Department of Physics and Astronomy, Ames Laboratory - U.S. Department of Energy, Ames, Iowa 50011, USA*
[3]*Department of Chemistry, Iowa State University, Ames, Iowa 50011, USA*
[4]*Department of Physics and Center for Nanointegration CENIDE, University of Duisburg-Essen, Lotharstrasse 1, 47057 Duisburg, Germany*

The realization of the unusual properties of two-dimensional (2D) materials requires the formation of large domains of single-layer thickness, extending over the mesoscale. It is found that the formation of uniform graphene on SiC, contrary to textbook diffraction, is signaled by a strong bell-shaped component (BSC) around the (00) and G(10) spots (but not around the substrate spots). The BCS is also seen on graphene grown on metals, because a single uniform graphene layer can be also grown with large lateral size. It is only seen by electron diffraction but not with x-ray or He scattering. Although the origin of such an intriguing result is unclear, its presence in the earlier literature (but never mentioned) points to its robustness and significance. A likely mechanism relates to the the spatial confinement of the graphene electrons, within a single layer. This leads to large spread in their wave vector which is transferred by electron-electron interactions to the elastically scattered electrons to generate the BSC.

I. INTRODUCTION

Graphene has been intensively studied as a novel two-dimensional (2D) material because of its unique band structure, with potential graphene applications predicted in many technologically important areas [1–4]. The key goal is to grow graphene of the highest quality, i.e., of uniform thickness, and lowest density of defects. Similar goals have become a current priority for the growth of other 2D van der Waals bonded materials with electronic band structures similar to graphene [5]. In this study we demonstrate a surprising result: Paradoxically a very broad bell-shaped component (BSC) emerges around both the specular (00) and the graphene G(10) spots, signaling the formation of a uniform layer. Although this component has been seen in numerous other experiments in the previous literature, it has been ignored and has not been correlated with graphene uniform growth [6–11]. The component's FWHM is as large as 50% of the surface Brillouin zone (BZ) and, since in diffraction broad peaks correspond to disorder, it is intriguing that it signals a high-quality uniform film. This conclusion is based on the unusual dependence of the BSC on electron energy found in the current experiments. They show that the BSC is not related to the scattering condition changing from constructive to destructive interference between adjacent terraces [12]. The fundamental nature of the effect is also seen for graphene grown on metals [13], with the BSC having similar characteristics [in this case only single-layer graphene (SLG) is possible]. Although the origin of the BSC is still not known, its intensity and presence in so many different growth experiments signals that it must be basic and universal. One possibility is that the BSC is a consequence of the graphene uniform thickness that confines the electrons with very high precision normal to the surface. As expected and as seen in angle-resolved photoemission spectroscopy (ARPES) experiments the spatial confinement causes a large spread in the normal component of the electron wave vector Δk_z [14], which possibly is transferred to the elastically diffracted electrons. The confinement extends coherently over mesoscale distances, since graphene is truly a unique, single-thickness film that overgrows substrate steps. The effect is unusually strong, fundamental, and general so that it should be present in other 2D van der Waals materials, of similar single-layer uniformity over the mesoscale [15].

II. EVOLUTION OF THE BSC IN GRAPHENE GROWTH EXPERIMENTS

The experiments were performed on $4H$-SiC(0001) purchased from Cree, Inc. The samples were graphitized in UHV ($P \sim 1 \times 10^{-10}$ Torr) by direct current heating of the sample to $\sim 1200°$–$1400\,°$C. Spot profile analysis low-energy electron diffraction (SPA-LEED) is used for the measurements, with its higher reciprocal-space resolution allowing quantitative analysis of the patterns [12]. Since elastically scattered electrons are collected within 0.5 eV below the beam energy, the BSC does not originate from plasmons [16] that involve higher energies [7]. The transition from the buffer to SLG is described in terms of the evolution of a small number of spots: the 6×6 spots around all fundamental spots and a three-spot cluster (close to the 1/3,1/3 position along [1$\bar{1}$00]). Figure 1 shows a 2D diffraction pattern of the surface partially covered with buffer layer (BL) and SLG. The spots in the cluster (the 5/13, along [1$\bar{1}$00] and the two neighboring spots along [1$\bar{2}$10]) are attenuated as graphene grows with further annealing. Since the BSC is not seen around the SiC spots, this implies that

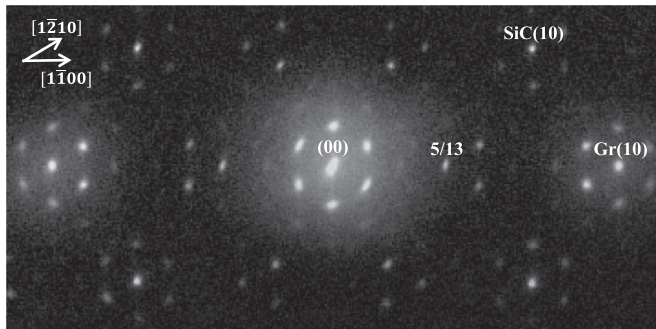*Corresponding author: mctringi@iastate.edu

FIG. 1. Diffraction pattern for mixture of BL and SLG at energy $E = 194$ eV. The BSC forms around the (00) and G(10) but not the SiC(10) spots. Several spots are marked including the 5/13 spot and the two neighboring spots forming a three-spot cluster. Its evolution tracks the transition from BL to SLG.

it originates from graphene electrons. Although the BSC and the spot evolution towards SLG were seen before [6–11], they were not discussed.

Graphene growth on the Si face of SiC is carried out at high temperatures (above $\sim$1200 °C) so Si evaporates while the remaining C diffuses and forms a uniform layer. Within a 200 °C window the grown thickness changes progressively from BL seen by the growth of $(6\sqrt{3} \times 6\sqrt{3})$, to single-layer, to bilayer, and multilayer graphene. The earlier work shows that the BSC evolves as the substrate changes from initial $(6\sqrt{3} \times 6\sqrt{3})$ to multilayer graphene. It starts appearing around the (00) spot after annealing to 1200 °C. With temperature increase, the 5/13 spot characteristic of the BL disappears (indicating the formation of SLG) while the BSC becomes stronger. Although the previous experiments have captured slightly different snapshots of the graphitization process, they are in agreement that BSC is a measure of graphene layer uniformity. Onset of the BSC around G(10) with $(\sqrt{3} \times \sqrt{3})$ and $(6\sqrt{3} \times 6\sqrt{3})$ phases coexisting is seen in Refs. [6,10]. More intense BSC is seen when the SLG forms, with the width of the BSC starting to decrease after bilayer [7] or graphite form [2] when the sample is heated to higher temperatures. The full evolution from BL to multilayer graphene studied in Ref. [8] shows that the width of the BSC is maximal in the middle of the temperature range, when SLG grows.

The correlation between strong BSC and high-quality graphene is also seen in Ref. [17]. The bottom profile shows the onset of graphitization (black curve at 1200 °C) and the top profile shows the completion of the SLG (green curve at 1300 °C). The BSC [shaded areas around (00) and G(10) spots] increases dramatically after SLG is completed. Quantitative analysis shows that the normalized area of the BSC grows three times around (00) spot, six times around the G(10), while the normalized area of the 5/13 (which measures the amount of BL present) decreases by a factor of 5. The electron energy is 194 eV and the normalization is over the total area of the profile.

The very presence of BSC is perplexing because graphene is the most uniform layer material. The trend of how the BSC evolves with temperature (or equivalently with thickness) is very consistent between these diverse papers. Since such samples of graphene on SiC (with BSC present) were

routinely used to characterize many fundamental properties of graphene, they show that the BSC correlates strongly with the highest-quality graphene [7,8,11]. The listed references [6–11] are only a small subset of many other similar studies. Concerning our samples (with maximal BSC), STM experiments have shown graphene domains reaching $\sim$5-μm sizes [18,11]. More recent characterization with three complementary techniques [SPA-LEED, scanning tunneling microscopy (STM), and ARPES] confirms the high quality of graphene from the presence of strong replica Dirac cones [19].

Further confirmation that the BSC is a general feature of graphene relates to its presence on graphene grown on metal surfaces, since this type of graphene is also highly uniform and overgrows steps. For growth on Ir(111), graphene forms by the thermal decomposition of ethylene above 1400 °C with dosing pressure of 5×10^{-6} mbar. Only the oriented $R0$ phase is present indicating highest quality of graphene. The BSC is similar (as for graphene on SiC) with FWHM $\sim$50% BZ, seen both around (00) and Ir(10) spots (Fig. 1 of Ref. [13]). A moiré pattern also forms with ten spots between (00) and Gr(10) (because $9a_{Ir} \approx 10a_g$). Because on this surface the graphene growth is along the Ir(111) unit cell (while on SiC it is rotated by 30° from the SiC direction), the BSC around Ir(10) is centered not on Ir(10), but on the Gr(10) spot. This confirms that graphene electrons are the cause of BSC [the G(10) rod is further away from (00) than the Ir(10) rod].

III. DIFFRACTION SPOT PROFILE ANALYSIS WITH ELECTRON ENERGY

Quantitative diffraction studies of surface morphology are routinely performed as a function of electron energy to measure the variation of spot profile shape, as it is decomposed into narrow and broad components [12]. At conditions of destructive interference the incoming and diffracted waves are out of phase with each other, which results in the broad component being maximal (and the narrow component minimal), while at conditions of constructive interference the reverse is true. From such studies to be described next we conclude that this is not the case and instead the narrow component and BSC are correlated in intensity, with their maxima (and also minima) at the same energies. These conclusions further confirm the unusual nature of the BSC. Such studies give the terrace and step height distributions statistically averaged over the area illuminated by the electron beam.

Figure 2(a) shows one-dimensional (1D) scans at $E = 148$ eV of the (00) spot [Fig. 2(a) along $[1\bar{2}10]$ and Fig. 2(b) at 132 eV along $[1\bar{1}00]$ with G(10) seen]. The high resolution of SPA-LEED is a clear advantage (over normal LEED) because it shows two distinct components of the (00) spot (while in Refs. [6–11] this is not possible). The narrow component has FWHM $= 0.5\%$ BZ, and the BSC has FWHM $= 33\%$ BZ. In textbook diffraction, broad spots commonly imply the presence of disorder and nonuniformity on the surface. However, the profiles of Fig. 2 are very unusual because the broad components have FWHMs, which correspond to a distance as small as $\sim 2a_g$, with $a_g = 0.245$ nm the graphene lattice constant. All studies of graphene with different probes have not identified any feature at this short length scale. Figure 2(b) shows the BSC around the two G(10) spots; the
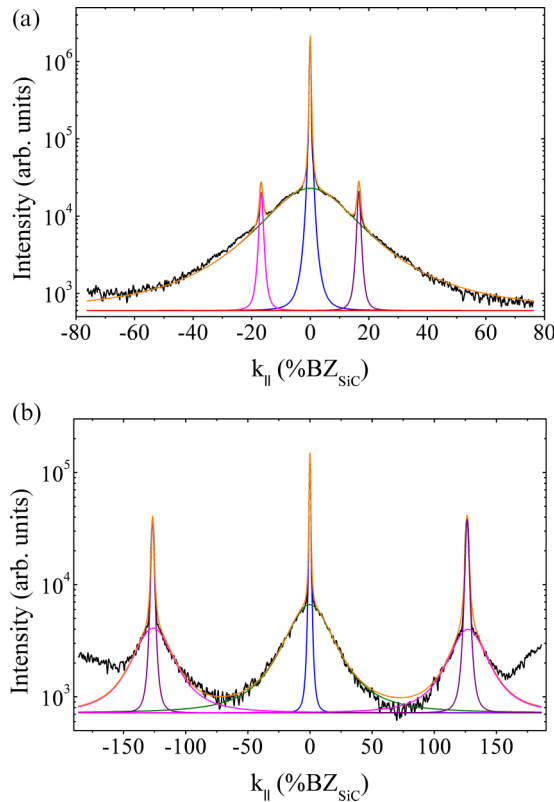
FIG. 2. (a) 1D scan of the specular spot along the SiC direction [$1\bar{2}10$]), at $E = 148$ eV. The FWHM of the narrow component is 0.5% BZ and of the BSC is 33% BZ which corresponds to a distance $\sim 3a_g$. The ratio of the integrated narrow component to the sum of narrow and BSC areas is ~ 0.65. (b) 1D scan of the specular along the graphene direction, and $E = 132$ eV. The FWHM of the G(10) narrow component is 2.25% BZ and of the BSC component is 80% of the FWHM of the (00) spot at the center of the scan. The integrated areas ratio of the narrow to the sum of the areas of both components is 0.5.

FWHM of the narrow component of G(10) is 2.25% BZ and the FWHM of the BSC of G(10) is smaller than the FWHM of the (00) spot at the center (by 20%).

Figure 3(a) shows in a pictorial way the spot profiles as a function of $k_{||}$ over a range of energies 100–200 eV. The intensity maxima are at 104, 144, and 200 eV, surprisingly at the same energies both for the narrow and BSC components; correspondingly the minima are at 124 and 160 eV again at the same energy for both components. This paradoxical result by itself suggests that the origin of the BSC is not related to changes of the scattering condition between adjacent terraces, from destructive to constructive interference [12]. If this was the case the narrow component should be anticorrelated to the BSC component, i.e., when the narrow component reaches a maximum (i.e., constructive interference) the broad component should reach a minimum (i.e., destructive interference). Figure 3(b) shows profiles of the G(10) spot as a function of energy over the same range. Maxima and minima are correlated to each other as for the (00) spot, although shifted to lower energy from the extrema of Fig. 3(a) by approximately 15 eV.
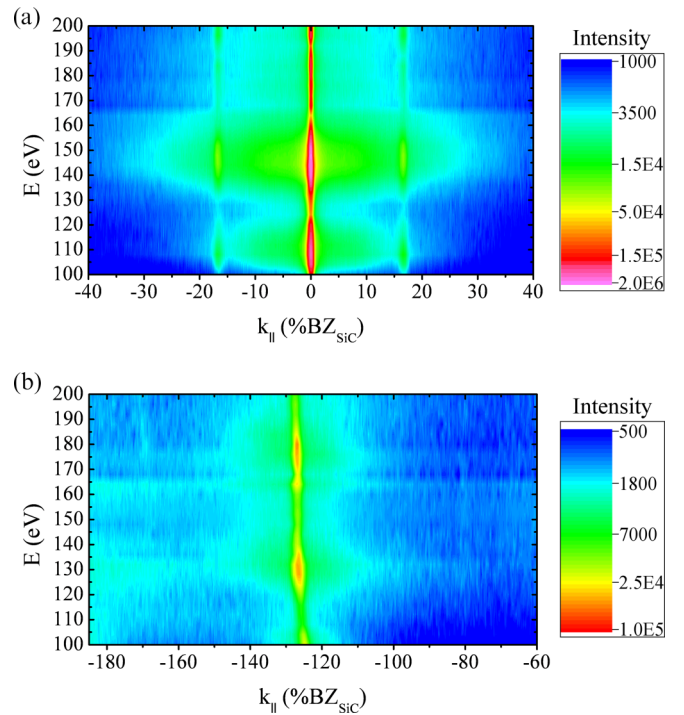

FIG. 3. (a) 1D profiles of the 00 spot collected every 4 eV from 100 to 200 eV. The color range is shown to the right (from 2×10^6 to 10^3). (b) 1D profiles of the G(10) spot collected every 4 eV from 100 to 200 eV. The color range is shown to the right (from 1×10^5 to 5×10^2). The maxima are shifted with respect to the maxima of the (00) in (a), because of the contribution of the nonzero parallel wavevector component of the G(10) spot. For both spots the maxima of the narrow and BSC components follow each other which is not consistent with scattering interference from adjacent terraces as the origin of BSC. [The initial bending of the Gr(10) spot is related to the nonlinearity of SPA-LEED at the edge of BZ and at lower energy.]

Figure 4 shows the integrated areas of the (00) narrow component A_{nar} (cyan), of the BSC background A_{bro} (blue) and their normalized ratios $R_{00} = A_{nar}/(A_{nar} + A_{bro})$, confirming again the correlation. The energy is shown in the top and the reduced variable $s = \Delta k_z / 2\pi / d_g$ at the bottom scale (where Δk_z is the momentum transfer normal to the surface). In addition the three maxima are close to half–integer values of $s = 5.5, 6.5, 7.5$, while if the BCS was due to scattering from adjacent terraces, the maxima of A_{nar} should be for integer values n so the phase shift s is $2n\pi$ [12].

IV. FURTHER CHARACTERIZATION AND ORIGIN OF THE BSC

Epi-graphene (EG) can be grown on either of the two polar faces of SiC, the SiC(000$\bar{1}$) (C face) or SiC (0001) (Si face). Graphene grown on the Si face of SiC is more uniform and extends to large lateral size. It has been extensively used to study its electronic and topological properties [2,3,20] and more recently to grow 2D materials by intercalation [21,22]. On the other hand graphene grown on the C face has a larger number of layers (more than ~ 10) and the domain sizes are smaller. The BSC is only seen on the Si-face graphene
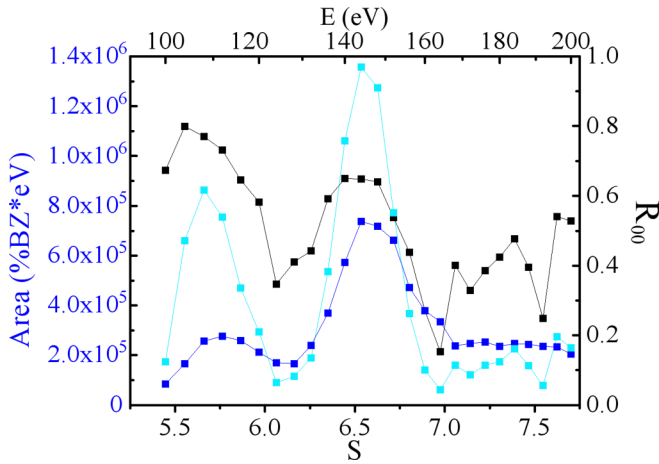
FIG. 4. Integrated areas of the narrow component (cyan) and the BSC (blue) plotted as a function of the scaled momentum transfer $s = (\Delta k_z)/(2\pi/d_g)$ (shown at the bottom, with the corresponding energy at the top). The two areas have the same variation with energy while they should be anticorrelated if the origin of BSC was textbook scattering. The fraction of the narrow component defined by the ratio $R_{00} = \frac{A_{nar}}{A_{nar}+A_{bro}}$ is plotted in black with the maxima close to half-integer values of $s = 5.5, 6.5, 7.5$. Maxima are expected for integer values of s if the BSC was originating from interference between adjacent terraces.

because of the larger domain size and single-layer thickness. No BSC is seen on the C phase of SiC, which confirms that less uniform morphology destroys the BSC [20].

A large number of diverse observations have been presented that show the BSC relates to the graphene single-layer uniformity, with the film extending without interruptions across terraces. A plausible physical mechanism generating the BSC which is related to such uniformity and can account for all observations can be electron confinement. The position of the graphene electrons is very precisely known within a single layer $d_g = 0.33$ nm, so they have a large variation in their wave vector normal to the surface, as determined by the uncertainty principle $\Delta k_z > 1/d_g$ (i.e., $\Delta p_z = \hbar/d_g$). The incoming electron beam primarily interacts with the atomic core (the atomic scattering factor is determined by the charge distribution of the protons in the C nucleus and the surrounding electron clouds in the C atoms). Electron-electron interaction between the incoming electron wave and the graphene valence electrons can also play a role (in the change of the electron wavelength due to the inner crystal potential and scattering resonances in the image potential, as discussed in scattering textbooks). Because of the elastic character ($E = $ constant) of the diffraction process (irrespective of whether the incoming beam interacts with graphene atoms or valence electrons) the undefined value of Δk_z in graphene electrons is transferred to the elastically scattered ones.

The spread Δk_z of the graphene electrons confined in graphene of uniform thickness can be transferred to the diffracted electrons during scattering via beam electron–graphene electron interactions. Because the scattering is elastic this can generate a spread to the parallel component $\Delta k_{||}$

of the scattered electrons which can be expressed

$$\Delta k_{||} = -k_z \Delta k_z/k_{||} = -(E - (h^2/2m_e)(k_{||}^2))^{1/2}(1/d_g)/k_{||},$$

$$(1)$$

where $(\Delta k_z, k_{||})$ define the spread of the momentum transfer for the spot under investigation and m_e the electron mass.

This type of scattering is unique to graphene (and not to other ultrathin films) because of the large continuous domains, which overgrow substrate steps, like a carpet. Graphene is the only system showing BSC. In all other cases films are interrupted at a step, which limits the spatial extent of the electron wave function in the film and the coherency in scattering between the incoming and valence electrons. As multilayer graphene of thickness nd_g grows with annealing, electron confinement is reduced and the FWHM $\Delta k_z \sim 1/nd_g$ decreases with n, consistent with the stronger BSC when SLG is grown.

A special growth study has shown how very large SLG domains can be grown under Ar pressure [4] that allows the growth to be performed at higher temperatures, which effectively increases the carbon diffusion length. Domains $\sim 50\,\mu$m long and at least $\sim 1\,\mu$m wide coexisting with 20% of bilayer graphene were grown. BSC is also seen on this optimal samples of very large lateral size. Typical SLG domain sizes in our experiments [11,18] and in Refs. [6–11] are $\sim 5\,\mu$m, a factor of 10 smaller. This suggests that the BSC is not sensitive to lateral size for very large domain sizes, but still highly sensitive to thickness uniformity. It is also an open question to determine this minimum lateral size required for a strong BSC to develop based on the confinement mechanism; this is more relevant for growth of graphene on metals where bare substrate and graphene covered areas usually coexist.

The proposed mechanism can explain more experimental observations in the literature about the dependence of the FWHM of the BSC on different parameters. As noted increasing $k_{||}$ at fixed E [i.e., comparing the G(10) vs the (00) spot], the FWHM decreases with $k_{||}$ as predicted from the smaller ratio $\Delta k_z/k_{||}$ for the graphene spot [in Eq. (1)]. With increasing beam energy E and for a given spot (so $k_{||}$ is fixed) the FWHM of BSC overall increases with energy, as expected from Eq. (1) [16].

More information can be obtained about the BSC by comparing scattering experiments using different probes. From the early graphene studies it was noted that x-ray-scattering on graphene grown on SiC shows only a single narrow component both on Si-and C-phase graphene as seen in Ref. [23]. Similarly, He-scattering experiments on graphene grown on Pt(111) also show one-component profiles with FWHM similar to the clean Ni(111) substrate [24]; this indicates that only long-range order is probed in the x-ray and He-scattering experiments and no BSC is present. The interaction between the graphene electrons (which have large Δk_z), with either the photons in the x-ray beam or the He atoms in the He beam, is much weaker so there is no transfer of this large momentum spread to the diffracted beam. Besides the LEED experiments on different types of graphene, the BSC has been also seen in experiments with μ-Low energy electron microscopy (LEEM) [25] and with reflection high-energy electron

diffraction (RHEED) [22]. μ- LEEM showing the variation of BSC with rotation was performed on graphene grown on Ir(111), for graphene domains of different orientations. The BSC was also seen in RHEED experiments studying superconductivity of intercalated graphene on SiC with Ca [22].

The BSC is a strong feature of graphene related to high-quality samples of uniform thickness. It would be of interest to search for the BSC in the growth of other 2D materials (which have not reached the high quality of graphene). Extending the role of BSC requires better understanding of a few issues: the dependence of BSC on lateral domain size (especially when separate islands of 2D materials are grown); domain orientation when there is a range of rotation angles depending on growth temperature; and how BSCs from areas of different thickness are added, if there is a distribution of different layers. These questions can be best answered from combined characterization with LEEM and area-selective μ- LEED.

V. CONCLUSIONS

In conclusion, an unusually broad background (BSC) seen in electron scattering experiments was studied quantitatively. Paradoxically it signals the formation of uniform graphene, contrary to textbook description that broad features in diffraction indicate disorder. Detailed studies of the diffraction profiles with energy rule out the standard analysis in terms of the variation of the scattering phase from constructive to destructive interference. The BSC is seen only around the (00) and G(10) spots but not around the SiC spots; it is seen only on the Si-face and not the C-face graphene because of larger, uniform domains grown on the former and it is seen for graphene grown on metals. BSC is not seen in x-ray or He-scattering scattering experiments. Its origin was attributed to the spatial localization of the graphene electrons, within a single layer, when uniform graphene is completed. This results in large spread in the wavevector normal to the surface $\Delta k_z > 1/d_g$ as a result of the uncertainty principle. This spread most likely is transferred to the elastically scattered electrons through electron-electron scattering, although details of the interaction require future theoretical work. The BSC most likely will be also present in other 2D systems of current interest, also signaling uniformity in their growth.

[1] K. S. Novoselov, A. K. Geim, S. V. Morozov, D. Jiang, Y. Zhang, S. V. Dubonos, I. V. Grigorieva, and A. A. Firsov, Science **306**, 666 (2004).

[2] C. Berger, Z. Song, T. Li, X. Li, A. Y. Ogbazghi, R. Feng, Z. Dai, A. N. Marchenkov, E. H. Conrad, P. N. First, and W. A. de Heer, J. Phys. Chem. B **108**, 19912 (2004).

[3] A. H. Castro Neto, F. Guinea, N. M. R. Peres, K. S. Novoselov, and A. K. Geim, Rev. Mod. Phys. **81**, 109 (2009).

[4] K. V. Emtsev, A. Bostwick, K. Horn, J. Jobst, G. L. Kellogg, L. Ley, J. L. McChesney, T. Ohta, S. A. Reshanov, J. Röhrl, E. Rotenberg, A. K. Schmid, D. Waldmann, H. B. Weber, and T. Seyller, Nat. Mater. **8**, 203 (2009).

[5] G. R. Bhimanapati, Z. Lin, V. Meunier, J. Yung, J. Cha, S. Das, D. Xiao, Y. Son, M. S. Strano, V. R. Cooper, L. Liang, S. G. Louie, E. Ringe, W. Zhou, S. S. Kim, R. R. Naik, B. G. Sumpter, H. Terrones, F. Xia, Y. Wang, J. Zhu, D. Akinwande, N. Alem, J. A. Schuller, R. E. Schaak, M. Terrones, and J. A. Robinson, ACS Nano **9**, 11509 (2015).

[6] P. Martensson, F. Owman, and L. I. Johansson, Phys. Status Solidi B **202**, 501 (1997).

[7] T. Langer, H. Pfnür, H. W. Schumacher, and C. Tegenkamp, Appl. Phys. Lett. **94**, 112106 (2009).

[8] C. Riedl, U. Starke, J. Bernhardt, M. Franke, and K. Heinz, Phys. Rev. B **76**, 245406 (2007).

[9] F. Owman and P. Martensson, Surf. Sci. **369**, 126 (1996).

[10] I. Forbeaux, J.-M. Themlin, and J.-M. Debever, Phys. Rev. B **58**, 16396 (1998).

[11] J. Hass, W. A. De Heer, and E. H. Conrad, J. Phys.: Condens. Matter **20**, 323202 (2008).

[12] M. Horn-von Hoegen, Zeitschrift Krist. **214**, 684 (1999).

[13] H. Hattab, A. T. N'Diaye, D. Wall, C. Klein, G. Jnawali, J. Coraux, C. Busse, R. van Gastel, B. Poelsema, T. Michely, F.-J. Meyer zu Heringdorf, and M. Horn-von Hoegen, Nano Lett. **12**, 678 (2012).

[14] T. Ohta, A. Bostwick, J. L. McChesney, T. Seyller, K. Horn, and E. Rotenberg, Phys. Rev. Lett. **98**, 206802 (2007).

[15] S. C. de la Barrera, Y.-C. Lin, S. M. Eichfeld, J. A. Robinson, Q. Gao, M. Widom, and R. M. Feenstra, J. Vac. Sci. Technol. B **34**, 04J106 (2016).

[16] S. Chen, M. Horn von Hoegen, P. A. Thiel, and M. C. Tringides (submitted to Carbon).

[17] See Supplemental Material at http://link.aps.org/supplemental/10.1103/PhysRevB.100.155307 for spot profiles along the [1$\bar{1}$00] direction showing onset of graphitization (black curve at 1200 °C) and after the completion of a SLG (green curve at 1300 °C). The BSC [shaded areas around (00) and G(10)] is stronger when SLG is completed. The green curve is shifted for clarity and the markers to the left scale show the same intensity at 650 counts. The relative contribution of the BSC to the integrated area over the shown BZ increases by a factor of 3, of the 5/13 decreases by a factor of 5, and of G(10) increases by a factor of 6 after annealing. This shows that the BSC correlates with the growth of SLG.

[18] M. Hupalo, E. H. Conrad, and M. C. Tringides, Phys. Rev. B **80**, 041401(R) (2009).

[19] L. Huang, Y. Wu, M. T. Hershberger, D. Mou, B. Schrunk, M. C. Tringides, M. Hupalo, and A. Kaminski, Phys. Rev. B **96**, 035411 (2017).

[20] K. V. Emtsev, F. Speck, Th. Seyller, and L. Ley, and J. D. Riley, Phys. Rev. B **77**, 155303 (2008).

[21] T. A. de Jong, E. E. Krasovskii, C. Ott, R. M. Tromp, S. J. van der Molen, and J. Jobst, Phys. Rev. Mater. **2**, 104005 (2018).

[22] S. Ichinokura, K. Sugawara, A. Takayama, T. Takahashi, and S. Hasegawa, ACS Nano **10**, 2761 (2016).

[23] W. A. de Heer, C. Berger, X. Wu, P. N. First, E. H. Conrad, X. Li, T. Li, M. Sprinkle, J. Hass, M. L. Sadowski, M. Potemski, and G. Martinez, Solid State Commun. **143**, 92 (2007).

[24] A. Tamtögl, E. Bahn, J. Zhu, P. Fouquet, J. Ellis, and W. Allison, J. Phys. Chem. C **119**, 25983 (2015).

[25] K. L Man and M. S Altman, J Phys.: Condens. Matter **24**, 314209 (2012).